inorganics

MDPI

Article

Impact of Iron-Bearing Fillers on the Mechanical Strength and Chemical Stability of Magnesium Potassium Phosphate Matrices Incorporating Rhenium

Sergey Sayenko [1,2,*], Volodymyr Shkuropatenko [1,2], Hans-Conrad zur Loye [3,*], Petr Vecernik [1], Monika Kiselova [1], Vlastislav Kašpar [1], Vlastimil Miller [1], Petr Bezdicka [4], Jan Šubrt [4], Petra Ecorchard [4], Natalija Murafa [4], Iva Milisavljevic [5] and Scott T. Misture [5]

1 ÚJV Řež, a. s., Nuclear Research Institute, Hlavni 130, 250 68 Řež, Czech Republic; v.shkuropatenko@ujv.cz (V.S.); petr.vecernik@ujv.cz (P.V.); monika.kiselova@ujv.cz (M.K.); vlastislav.kaspar@ujv.cz (V.K.); vlastimil.miler@ujv.cz (V.M.)
2 KIPT, Kharkov Institute of Physics and Technology, 1 Akademichna Str., 61108 Kharkiv, Ukraine
3 Department of Chemistry and Biochemistry, University of South Carolina, 631 Sumter Street, Columbia, SC 29208, USA
4 Institute of Inorganic Chemistry of the Czech Academy of Sciences, Husinec-Řež 1001, 250 68 Řež, Czech Republic; petrb@iic.cas.cz (P.B.); subrt@iic.cas.cz (J.Š.); ecorchard@iic.cas.cz (P.E.); murafa@iic.cas.cz (N.M.)
5 Kazuo Inamori School of Engineering, Alfred University, Alfred, NY 14802, USA; im6@alfred.edu (I.M.); misture@alfred.edu (S.T.M.)
* Correspondence: sergii.saienko@ujv.cz (S.S.); zurloye@mailbox.sc.edu (H.-C.z.L.)

Abstract

We report on the study of the immobilization process of non-radioactive rhenium (Re), a chemical analogue of technetium-99 (^{99}Tc), in compounds based on magnesium potassium phosphate (MKP), as well as the possibility of enhancing their properties with iron-bearing additives/fillers. Powdered Re_2O_7 was used as the initial Re-containing source. Because of the solubility and high leachability of Tc (VII), which is also volatile at high temperatures, its immobilization for long-term storage and disposal poses a serious challenge to researchers. Taking this into account, low-temperature stabilization technology based on MKP, a cementitious material, is currently considered promising. We prepared experimental specimens based on Re-incorporated MKP matrices and analyzed their microstructure in detail using analytical methods of X-ray diffraction (XRD), Raman spectroscopy, scanning electron microscopy (SEM), and transmission electron microscopy (TEM). Considering that iron-bearing substances can reduce Tc (VII) to the lower-valence form Tc (IV), which is more stable, attention was also paid to evaluate the effect of fillers (Fe_2O_3, Fe_3O_4, Fe, FeS and blast furnace slag (BFS)) on strength, oxidation state, and water resistance (expressed as leaching cumulative concentration). The addition of fillers ensures the formation of denser compounds based on MKP after 28 days of curing under ambient conditions and increases their mechanical strength. The oxidation state of Re and the reduction from Re (VII) to Re (IV) was estimated using X-ray-absorption near-edge structure (XANES) analysis. Considering the Re leaching concentrations from tests using the ANS-16.1 standard in water, enhanced leachability indices (LI) for Re from MKP matrices were determined with the addition of iron-bearing fillers. Overall, the average LI values were greater than the minimum limit, indicating their acceptance for disposal recommended by the U.S. Nuclear Regulatory Commission.

Keywords: radioactive waste immobilization; technetium; rhenium; magnesium potassium phosphate; matrix; phase composition; microstructure; oxidation state; strength; leaching

Check for updates

Received: 1 December 2025
Revised: 19 January 2026
Accepted: 24 January 2026
Published: 28 January 2026

Copyright: © 2026 by the authors. Licensee MDPI, Basel, Switzerland. This article is an open access article distributed under the terms and conditions of the Creative Commons Attribution (CC BY) license.

1. Introduction

Technetium (Tc) and the most abundant Tc isotope, ^{99}Tc from liquid radioactive waste stored in various tanks (such as at the Savannah River site and Hanford site) and decommissioned wastes, are hazardous radionuclides that pose a serious threat to the environment. The wide variation and complex chemistries of liquid nuclear waste streams containing ^{99}Tc create specific challenges on mechanical strength and chemical stability when immobilizing the waste in materials/matrices suitable for long-term storage and disposal.

The high environmental risk associated with Tc is due to its long half-life (2.1×10^5 years) and the high mobility of the oxidized anionic species $Tc(VII)O_4^-$ in which technetium can exist once introduced into the environment. Under reducing conditions, Tc (VII) is reduced to Tc (IV) as hydrous Tc oxide ($Tc(IV)O_2 \cdot nH_2O$), which is relatively insoluble and immobile [1,2]. Therefore, if Tc (VII) is reduced to more stable Tc (IV) by natural or synthetic reducing agents, immobilizing ^{99}Tc becomes more feasible [3]. Recent work [4–11] has revealed that absorbers of Fe and Fe-bearing oxides are effective matrices using reduction of TcO_4^- from Tc (VII) to Tc (IV) via reductive adsorption or precipitation.

For decades, various waste forms, including glass, ceramics, and cementitious materials, have been tested and used for solidification, immobilization, and retention of ^{99}Tc, as reviewed in [12,13]. In several studies, rhenium (Re) has been used as a preferred non-radioactive surrogate for ^{99}Tc due to its similar speciation, ionic size, and hydration energy [14–17].

Among various sequestration methods, since the volatilization and boiling points of ^{99}Tc are 311 °C and 900 °C [18], respectively, low-temperature immobilization processes (cementing) are of the greatest interest. However, cementation is complicated by the fact that technetium in a cement compound in the oxidized form Tc (VII) is easily leached [19]. One approach to improve technetium retention is to use a reducing grout waste form, for example, when blast furnace slag and fly ash are added [20].

In the last few decades, Portland cement has been the primary cementitious material in various fields of application. However, its production involves significant CO_2 emissions [21]. In light of the foregoing facts, there would appear to be little doubt that alternative binders less aggressive to the environment must (at least partially) replace Portland cement [22].

Magnesium phosphate cements represent a class of inorganic "low-CO_2" cements that have garnered considerable interest in recent years for their superior performance in environmental protection and energy conservation compared to traditional Portland cement and have diverse applications in the construction and engineering sectors [23]. One of their most interesting applications is in the immobilization of radioactive waste [24]. Magnesium phosphate cements based on the ($MgO–PO_4^{3-}–H_2O$) system, are mainly formulated from calcined magnesium oxide, phosphate, and retarder and other mineral admixtures in certain proportions, representing a cementitious system different from ordinary cement [25].

Magnesium potassium phosphate (MKP) cement, one of the environmentally friendly binders with broad prospects, is a clinker-free acid–base cement in which mechanical strength development is a direct result of the rapid formation of cementitious hydrogel-type products [26,27]. The chemical reaction resulting in the formation of MKP cement binder (Equation (1)) is based on the dissolution of MgO and KH_2PO_4 reacting in solution to form magnesium potassium phosphate, which is isostructural to struvite ($NH_4MgPO_4 \cdot 6H_2O$) [28] and is naturally cementitious [29].

$$MgO + KH_2PO_4 + 5H_2O \rightarrow MgKPO_4 \cdot 6H_2O + Q \quad (1)$$

The reaction product is MKP, struvite K (magnesium potassium phosphate hexahydrate $MgKPO_4 \cdot 6H_2O$), which sets at room temperature to form a crystalline material [28,30,31]. The MKP cement-based waste form can be used to treat solids, liquids, and sludges by chemical immobilization, microencapsulation, and/or macroencapsulation [30]. When compared to conventional Portland cements, MKP cement is a potential magnesia-based cementitious material that has advantageous properties, including near-neutral pH, low water demand, low drying shrinkage, and high early compressive strength [32]. In references [29,33,34], it was demonstrated that fillers/aggregates of iron/iron oxides can improve the compressive strength and water resistance of a solid MKP-based matrix. MKP cement, with its strong and dense matrix, has excellent pollutant binding capacity, making it a candidate for macroencapsulation.

An MKP-based compound called Ceramicrete, described as a chemically bonded phosphate ceramic (CBPC), is a relatively new engineering material developed at Argonne National Laboratory to stabilize radioactive and hazardous waste streams [31,35,36]. MKP cements have been widely proposed and studied to treat various real nuclear wastes in the United States and Russia, including waste containing technetium radioactive elements [30,37–39]. In [40], Ceramicrete, was used to solidify liquid waste containing ^{99}Tc. $SnCl_2$ (2–3 wt.% of binder mix) as a reducing reagent for the reduction of Tc (VII) to Tc (IV). To improve the structural integrity of the final waste form, fly ash (38 wt.% of the total content of the binder powder mixture) was added. These waste forms demonstrated compressive strength of approximately 30 MPa and were highly resistant to aqueous media. In [41], specimens of Ceramicrete composition containing goethite (α-FeO(OH)) were proposed and tested for the ability to stabilize residual waste containing ^{99}Tc from the C-202 tank at Hanford. Leaching tests in water showed a positive effect: the addition of goethite to the stabilization matrix based on Ceramicrete reduced the release of technetium from 29% to 5.8%–6.3% of the total. Reference [42] is devoted to the selection of modifiers of various types to increase the stability of technetium in MKP during the immobilization of technetium-containing waste, in which various fillers were considered, including iron-containing ones.

In view of the above, as well as having experience in conducting joint research by partners from the USA, Ukraine, and the Czech Republic on studying magnesium potassium phosphate materials [43–45], we demonstrate the process of low-temperature stabilization of Re, a Tc surrogate, in MKP-based matrices. Our research was aimed at exploiting the synergy between an MKP-based matrix containing Re and additives (Fe_2O_3, Fe_3O_4, Fe, FeS, and BFS), which can improve its physical properties and chemical stability.

2. Results and Discussion

2.1. Characterization of MKP Matrices Incorporating Rhenium

The phase composition of all investigated MKP–Re specimens was studied using XRD analysis. XRD patterns of MKP-based specimens without and with the addition of Re_2O_7 are shown in Figure 1.

As can be seen in Figure 1a and based on the calculated data on the quantitative content of phases in accordance with the standard Rietveld method, the MKP compound consists of two phases—K-struvite ($MgKPO_4 \cdot 6H_2O$) 77% and periclase (MgO) 23%—which indicates the presence of unreacted particles of MgO powder. The lattice parameters of K-struvite are presented in Table 1.

The addition of 5% Re_2O_7 leads to changes in the phase structure of MKP: in addition to K-struvite (77%) and periclase (16%), a new phase appears—potassium perrhenate or potassium rhenium oxide ($KReO_4$) with a content of 7% (Figure 1b). In this case, the lattice parameters of K-struvite slightly increased with a corresponding increase in the unit cell

volume (ΔV = 0.13%) compared to pure MKP. This fact may indicate partial inclusion of rhenium in the crystal lattice of K-struvite, given its ability to undergo numerous substitutions [46]. Quantitative analysis using the Rietveld method revealed a decrease in the amount of unreacted MgO from 23% to 16%, which is associated with an increase in the acidity of the medium due to the dissolution of Re_2O_7. However, the amount of K-struvite did not change significantly.

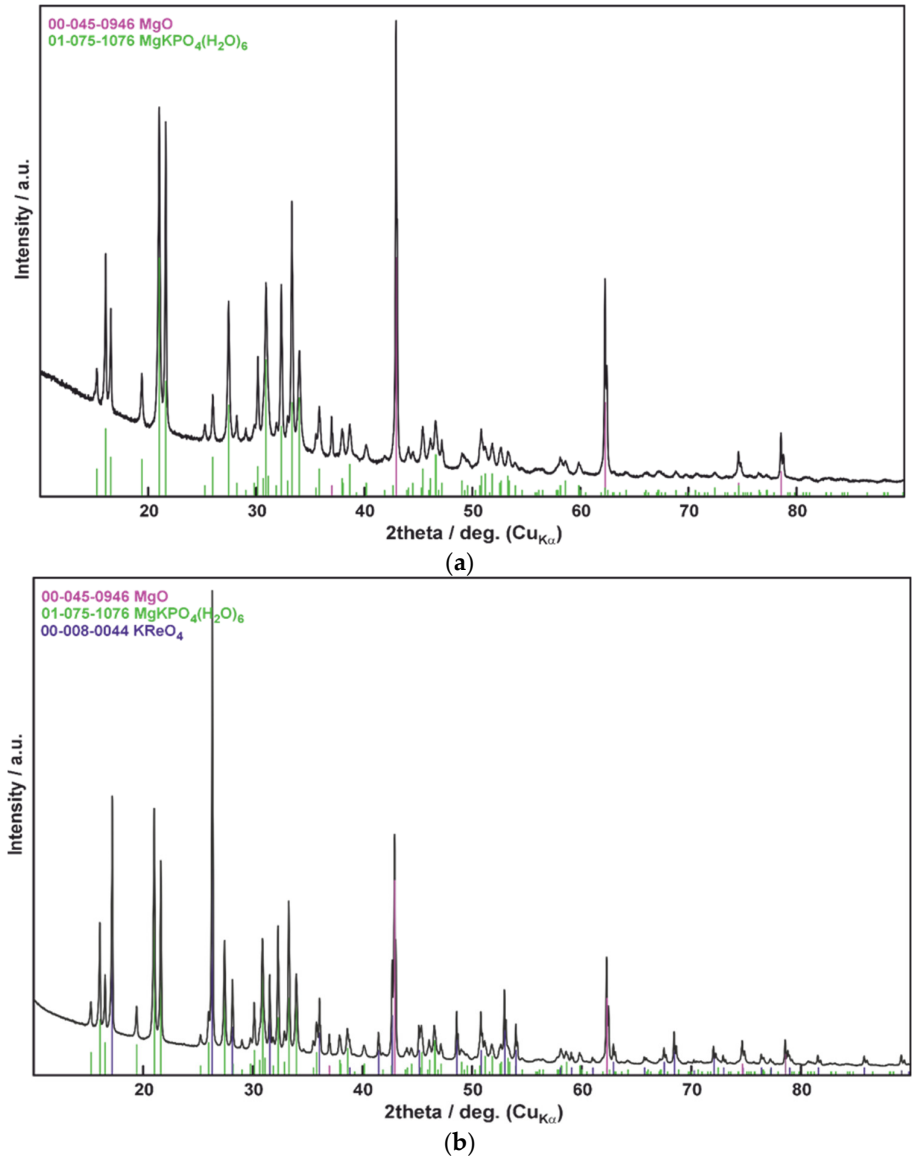


Figure 1. XRD patterns of the solid specimens after 28 days of curing: MKP (**a**) and MKP–Re (**b**).

Table 1. Unit cell parameters of the MKP specimens.

Specimen	Unit Cell Parameters			
	a/nm	b/nm	c/nm	V/nm^3
MKP	0.68751 (2)	0.61631 (2)	1.10942 (3)	0.470082
MKP–Re	0.68795 (1)	0.616512 (1)	1.10979 (1)	0.470695

As is known, in the process of obtaining the MKP compound according to Equation (2), KH_2PO_4 is mixed with water and its further dissolution occurs, in accordance with Equation (3).

$$KH_2PO_4 \rightarrow K^+ + H_2PO_4^- \quad (2)$$

In turn, the added Re_2O_7 powder also dissolves in the aqueous medium, forming ion ReO_4^-. Further, because of the reaction (Equation (3)), $KReO_4$ is formed.

$$K^+ + ReO_4^- \rightarrow KReO_4 \quad (3)$$

The Raman spectra of pure MKP, MKP with the addition of 5% Re_2O_7 (MKP–Re), and initial rhenium oxide powder are shown in Figure 2. The Raman spectra of MKP and MKP–Re specimens clearly shows peaks at 228, 426, 462, 562, and 943 cm^{-1}, characteristic of K-struvite. Also, Raman bands are observed in the 3000-wavenumber range, corresponding to stretching vibrations of water [47]. The peak near 295 cm^{-1} corresponds to MgO [48]. These data confirm the results of XRD analysis on the presence of the main phase, K-struvite, in the MKP matrix, as well as the presence of MgO (Figure 1).

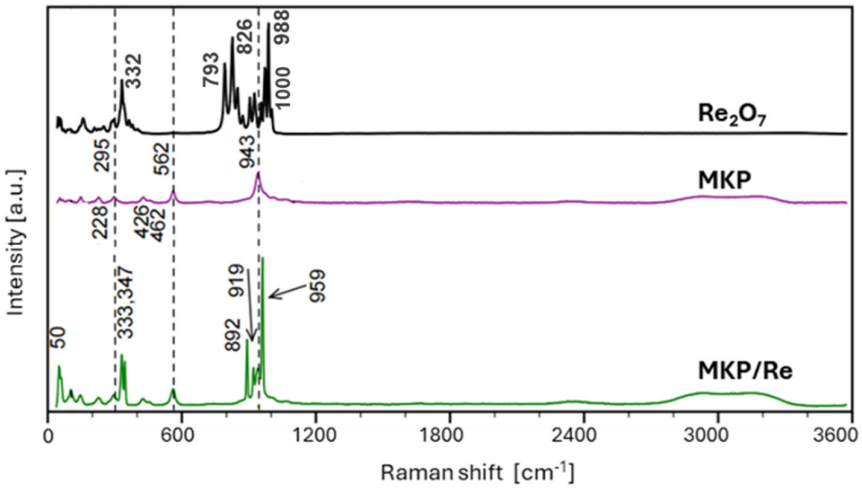


Figure 2. Raman spectra of specimens: Re_2O_7, MKP, and MKP–Re.

The remaining peaks at 50, 333, 347, 892, 919, and 959 cm^{-1} in the Raman spectrum of the MKP–Re specimen belong to potassium perrhenate ($KReO_4$), the presence of which is also indicated by XRD data (Figure 1b). In [49], the following characteristic peaks for $KReO_4$ are given: 49, 335, 893, 910, and 969 cm^{-1}. As can be seen in Table 2, the Raman peaks of $KReO_4$, found in the MKP–Re composition, differ from the values given in this work by the presence of a peak at 347 cm^{-1} and a shift of ~10 cm^{-1} of the peaks at 919 and 959 cm^{-1}.

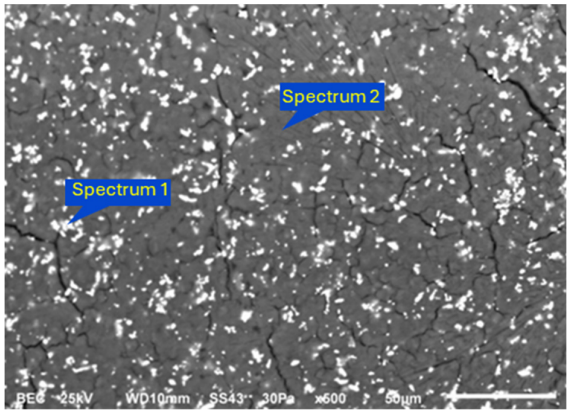
Table 2. Raman spectroscopy data for K-struvite and $KReO_4$.

Raman Modes of Struvite (cm^{-1})		Raman Modes of $KReO_4$ (cm^{-1})	
Observed	**Ref. [47]**	**Observed**	**Ref. [49]**
		50	49
228	228.5		
		333	335
		347	-
426	427.5		
462	462.8		
562	564.1		
		892	893
		919	910
943	941.8		
		959	969

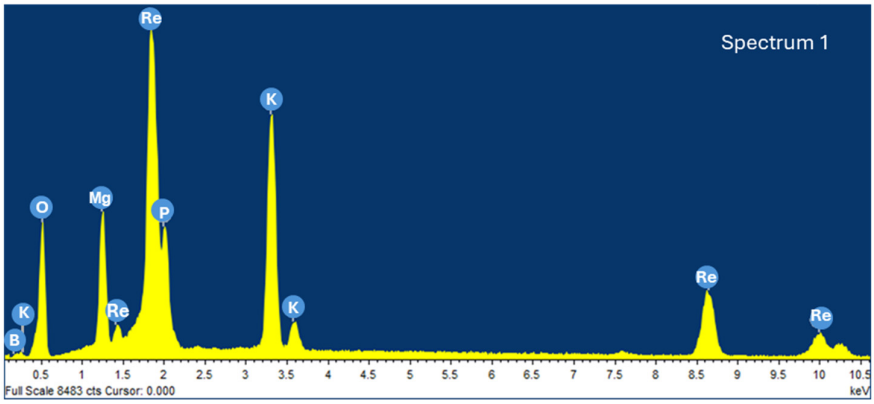
The detected peaks in the Raman spectrum for Re_2O_7 powder—332, 793, 826, 988, and 1000 cm^{-1}—are close to the peaks for crystalline Re_2O_7 determined by the authors of

reference [50]. The absence of the peaks characteristic of Re_2O_7 in the Raman spectrum for the MKP–Re compound indicates that Re_2O_7 has completely dissolved and reacted to form $KReO_4$.

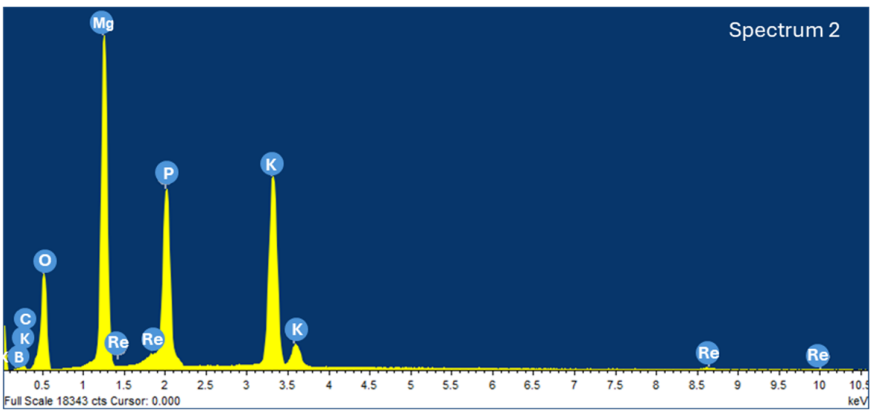
Fractured sections of freshly broken pieces of MKP–Re after 28 days of curing were analyzed using SEM. Many light particles surrounded by a dark matrix were detected (Figure 3a).



(**a**)



(**b**)



(**c**)

Figure 3. SEM images of the MKP-Re specimen: (**a**) microstructure, (**b**) EDS spectrum of light particles, (**c**) EDS spectrum of the matrix.

EDS analysis of the light particles (spectrum 1, Figure 3b) shows the presence of stronger peaks of Re, K, and O, indicating that these particles are composed of $KReO_4$. Small, light $KReO_4$ particles (no more than 5 µm) are characterized by a broad size distribution, are unevenly distributed in the matrix, and are prone to aggregation, which is consistent with reference [51]. Spectrum 2 (Figure 3c) of the matrix material shows intense peaks of

Mg, K, P, and O, indicating the presence of magnesium potassium phosphate (K-struvite $MgKPO_4 \cdot 6H_2O$).

Based on the elemental maps (Figure 4), uniform distribution of K, Mg, and P is observed throughout the matrix, consistent with the formation of crystalline K-struvite as the main binding phase of the system. The presence of areas (or clusters of Mg-containing particles) with elevated Mg content is associated with the presence of embedded unreacted MgO particles, which is consistent with the XRD data in Figure 1b.

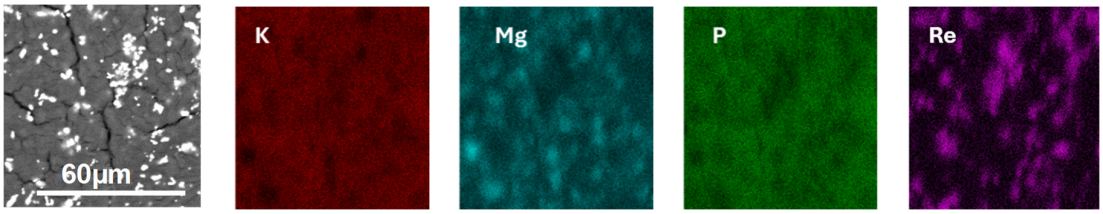


Figure 4. Elemental maps of MKP–Re specimen after 28 days of curing.

The solid MKP–Re specimen was ground into particles and analyzed using a transmission electron microscope (Figure 5).

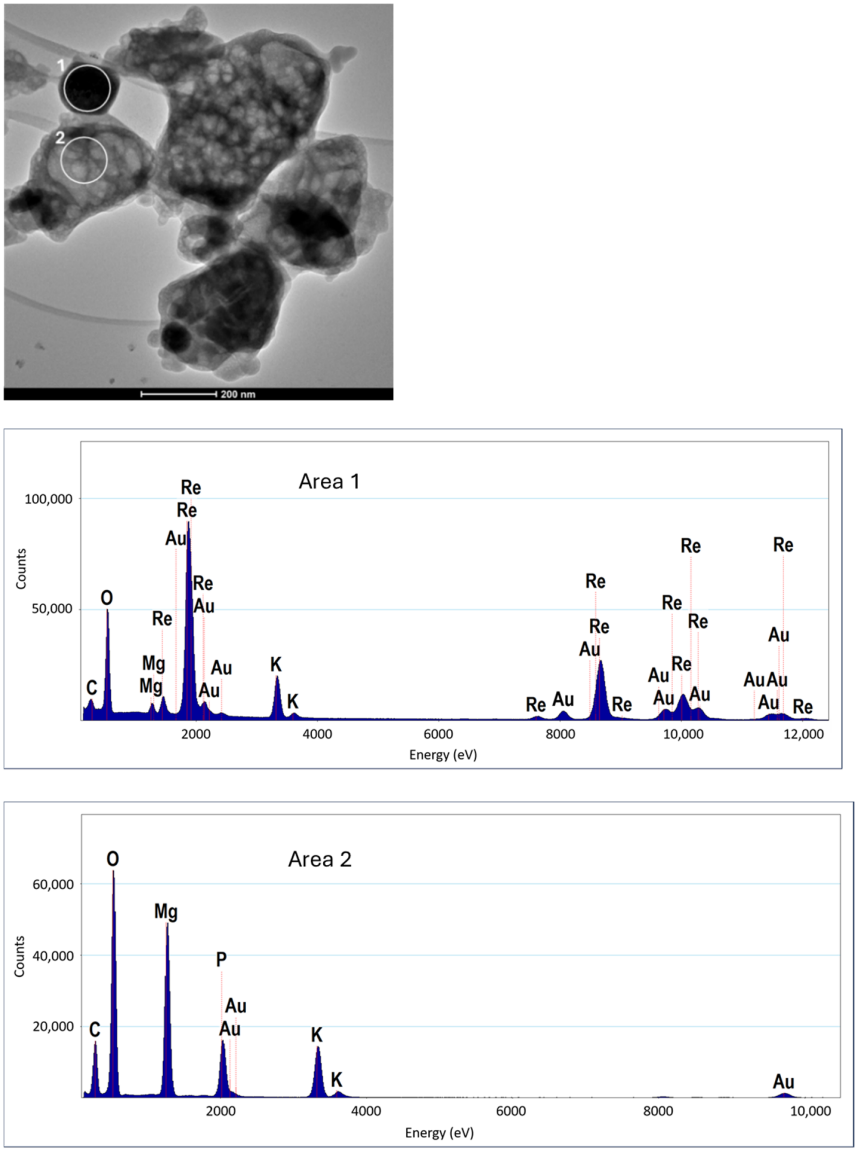


Figure 5. TEM image and EDS spectra of the particles of MKP–Re specimen.

In area 1, a dark, spherical particle ~150 nm in size consisting of $KReO_4$ is clearly visible. This is indicated by the presence of stronger peaks of K, Re, and O in the EDS spectrum of region 1. Peaks of Au and C are associated with target materials containing specimens for TEM analysis. As can be seen, the $KReO_4$ particle is associated with particles of the MKP matrix, which are combined into agglomerates. Large agglomerates ~500 nm in size include small particles of the MKP matrix, 10–30 nm in size. In area 2, EDS data indicate the presence of the major components of K-struvite, namely Mg, K, P, and O.

Thus, using XRD, Raman spectroscopy, SEM/EDS, and TEM/EDS analysis of the MKP-based compound, it was established that in the case of incorporation of powdered Re_2O_7 oxide (5 wt.%), the resulting matrix contains, in addition to K-struvite and unreacted MgO, potassium perrhenate $KReO_4$. SEM and TEM observations showed that $KReO_4$ was present in the form of particles of various sizes, embedded in the MKP matrix.

2.2. Properties of MKP-Based Matrices Incorporating Re Obtained Using Iron-Bearing Additives

2.2.1. Compression Strength

Mechanical strength tests of MKP-based specimens with different Fe-containing fillers were carried out after 1, 7, and 28 days of curing, and the results are presented in Figure 6. For all specimen proportions, there were three replications of each measurement and their average value was taken as the value of strength. The difference between the maximum deviation of the measured strength value and the average strength is expressed on the graph as the standard deviation.

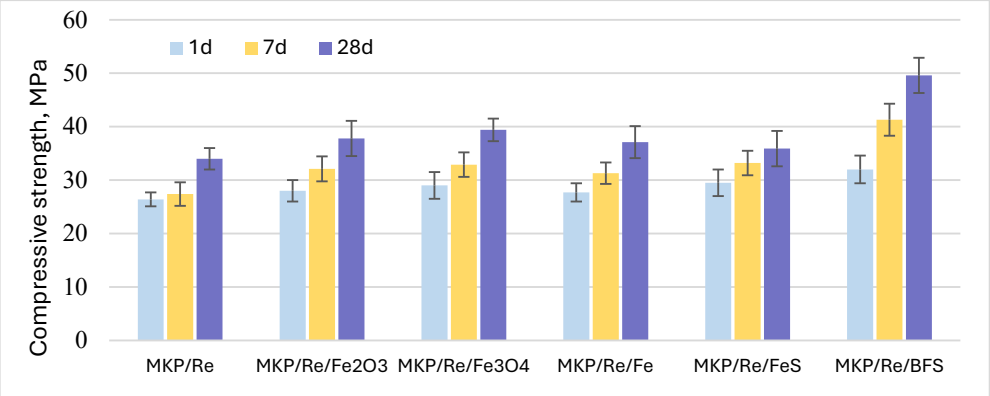


Figure 6. Compressive strength of MKP compounds with additions Fe_2O_3, Fe_3O_4, Fe, FeS, and BFS.

The mechanical strength of the pure MKP compound without additives was 37.2 MPa. The addition of rhenium oxide led to a decrease in strength due to the formation of $KReO_4$ (according to XRD analysis, Figure 1b), which is shown in Figure 6 for the MKP–Re specimen (34 MPa). The compressive strength of the MKP-based specimens incorporating 5% Re_2O_7 increased with the addition of fillers for all curing periods. The maximum compressive strength after 28 days reached 49.6 MPa for the specimen with BFS added. The addition of 10 wt.% BFS increased strength by 46% compared to the initial MKP–Re specimen.

Different countries have set their own values for waste acceptance criteria (WAC), namely the minimum compressive strength required for the acceptance of cementitious waste forms at a radioactive waste disposal facility. In the USA, the WAC compressive strength is 500 psi or 3.45 MPa [52], almost the same as the 3.44 MPa in South Korea [53], and in European research projects to develop novel cementitious materials, a value of 5 MPa is currently used [54].

Our findings that BFS additives contribute to the highest mechanical strength of the MKP matrix have been confirmed by other researchers. Gardner et al. [29] conducted a study of the structure and characteristics of MKP-based materials with the addition of

50 wt.% BFS, and a significant increase in the compressive strength after 28 curing period from 22 MPa to 34 MPa was shown. In [55], it was shown that a compressive strength of 21.6 MPa was achieved for an MKP compound with BFS added (28.33 wt.%). According to reference [33], the addition of BFS enhanced the early mechanical performance of MKP mortar due to both the physical filler effect and chemical reaction.

One common explanation for the increased compressive strength of MKP with the addition of BFS is related to the chemical composition of this additive. BFS is rich in reactive forms of SiO_2 and Al_2O_3, which are in an amorphous or slightly crystalline phase, making them readily available for dissolution in the alkaline-salt environment of MKP. As a result of the reaction of silicon and aluminum, additional aluminosilicate phases are formed [29,33]. The secondary products forming in MKP blended with BFS are highly enriched in Al and Si, which could potentially lead to the formation of a potassium aluminosilicate phases that may enhance overall densification and potentially increase the durability of MKP binders. In [56], this reaction made the bridging structure different from the struvite or K-struvite structure formed in the system, which caused more connections between the magnesia particles, and the overall structure was more compact.

The compressive strength values of the MKP specimens presented in Figure 6 exceed the WAC requirements for cement matrices. Unlike the BFS additive, the addition of Fe_2O_3, Fe_3O_4, Fe, and FeS slightly increases the compressive strength of MKP. The authors of this article previously showed [8] that the addition of Fe_2O_3 and Fe_3O_4 to the MKP system does not cause the formation of new crystalline phases and that these oxides do not enter into chemical interaction, but act as inert fillers. Apparently, Fe and FeS also have only a physical effect as fillers on the strength properties of the MKP matrix.

2.2.2. Re Oxidation State

Because leaching of Tc is strongly dependent on its oxidation state [41], it was important to estimate the redox conditions of the Re as Tc surrogate in the MKP matrix for reducing Re from the (VII+) to the (IV+) valence insoluble oxidation state in the presence of the reducing agent, such as Fe_2O_3, Fe_3O_4, Fe, FeS, and BFS. The characteristic Re L_3 edge XANES spectra are illustrated in Figure 7, and the edge positions are presented in Table 3. In all cases, edge energy is obtained from the position of the zero crossing of the second derivative. The spectra look like high-oxidation-state Re (VII) with some reduced Re. The edge position for Re in the MKP–Re–Fe_2O_3 specimen is 10,543.87 eV, while for MKP–Re–FeS it is 10,545.27 eV, a difference of 1.4 eV. As is known [57], the L_3 edge gives an estimation of the oxidation state. In a general sense, the height of the white line is defined by electron localization, and as the oxidation state changes (partially) to lower oxidation states, the white line becomes less pronounced and the edge position shifts. Thus, the data can be interpreted as Re (VII), and for the specimens with some reduction, then the data show a mix of oxidation states—possibly (VI) and/or (IV) mixed with (VII). The general trend in reduction state is: FeS (most reduced), BFS, Fe, Fe_3O_4, Fe_2O_3 (least reduced).

Table 3. Position of Re L_3 edge peaks in XANES spectra.

Specimen	Edge Energy (E_0) *
MKP–Re–Fe_2O_3	10,543.9
MKP–Re–Fe_3O_4	10,544.0
MKP–Re–Fe	10,544.7
MKP–Re/BFS	10,545.0
MKP–Re–FeS	10,545.3

* Edge energy obtained from the position of the zero crossing of the second derivative.

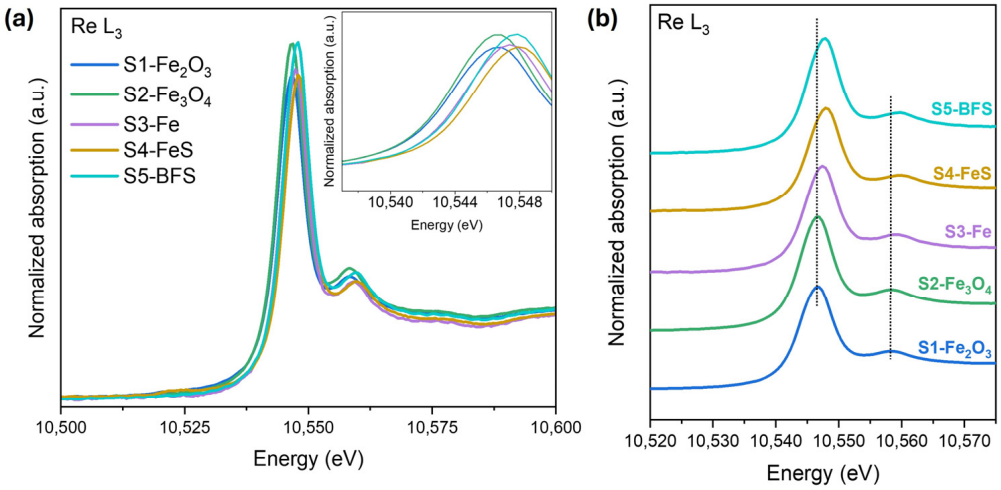


Figure 7. Results of the XANES study: (**a**) Re L_3 XANES spectra in the different MKP-based compounds with Fe_2O_3, Fe_3O_4, Fe, FeS, and BFS additives; (**b**) expanded view of the Re L_3 absorption edge, highlighting systematic shifts in the white line position as a function of the additive.

2.2.3. Leaching Behavior

The data from leaching tests of MKP specimens in accordance with the ANSI/AN16.1 standard [58] are presented as dependencies of the leaching cumulative concentrations (C_c) of Re (Figure 8). Comparing the C_c of Re from pure MKP compound and with fillers, it is clearly evident that the addition of fillers leads to a decrease in its value. This can be explained by the presence of locally reducing conditions for Re (VII) arising from the presence of iron ions in the fillers, as confirmed by XANES data (Figure 7, Table 3). In the case of iron-bearing fillers, Re is leached to the greatest extent from the MKP matrix with the addition of Fe_2O_3. Leaching decreases with the addition of Fe_3O_4, Fe, FeS, and BFS, with the lowest cumulative concentration.

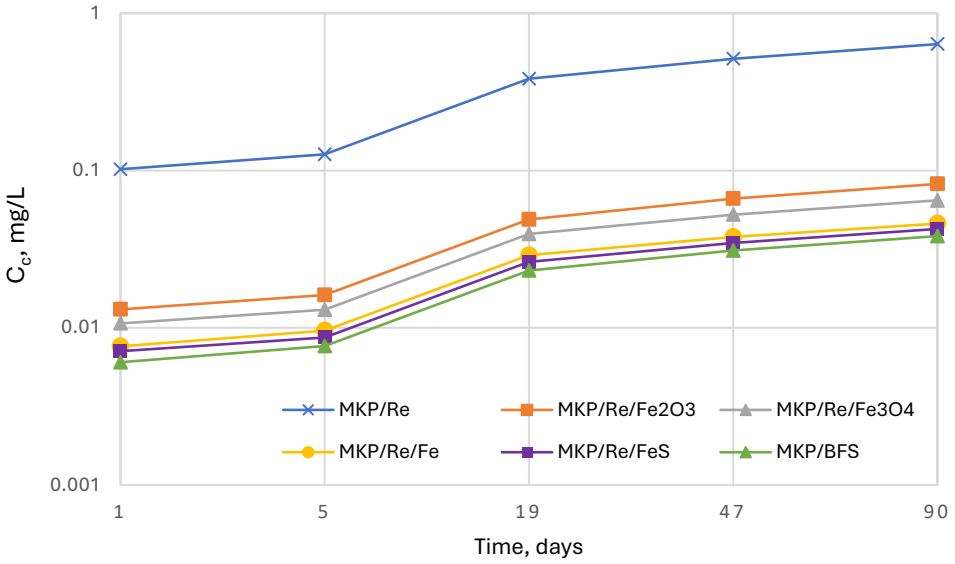


Figure 8. Re leaching cumulative concentrations from MKP-based specimens with addition of Fe_2O_3, Fe_3O_4, Fe, FeS, and BFS.

The effective diffusion coefficients (D_e) and the corresponding leachability indices (LI) for Re were calculated using Equations (4)–(6) for the MKP-based specimens and are given in Table 4.

Table 4. Calculated effective diffusion coefficients (D_e) and leaching indices (LI) for Re.

Specimen	MKP–Re	MKP–Re–Fe_2O_3	MKP–Re–Fe_3O_4	MKP–Re–Fe	MKP–Re–FeS	MKP–Re–BFS
D_e (cm^2/s)	1.14×10^{-8}	4.36×10^{-9}	2.64×10^{-9}	1.45×10^{-9}	1.10×10^{-9}	8.94×10^{-10}
LI	8.20	8.62	8.87	9.13	9.26	9.31

The obtained data showed that D_e values ranged from 1.14×10^{-8} cm^2/s for MKP without filler to 8.94×10^{-10} cm^2/s with the addition of BFS. The XANES results above generally support the hypothesis that reduction reduces leachability. The values of all obtained LIs are above the WAC for radioactive waste forms to be disposed of at controlled sites, which should be at least 6.0 [59]. The higher the LI and the lower the D_e, the worse the leaching of the pollutant from the matrix. It should be noted that higher targets have been set for technetium (^{99}Tc) than the 6.0 value, namely LI > 9 ([37], page iv), based on early waste-disposal risk and performance assessment analyses.

Filler additions improve resistance to Re leaching, as evidenced by increased LI values. The addition of hematite (Fe_2O_3) increases LI values from 8.20 to 8.62, while magnetite (Fe_3O_4) increases them to 8.87, although they remain below the target level (LI > 9). LI values > 9 were observed for MKP with additions of metallic iron (Fe), iron sulfide (FeS), and BFS. The presented results clearly demonstrate improved rhenium retention with the addition of BFS (LI = 9.31). This means that Re (and therefore Tc also) is better retained in the MKP matrix with BFS filler than in the other MKP specimens considered. As is known, BFS contains both ferrous ion and sulfides, which are strong reductants for ^{99}Tc to enhance the immobilization of ^{99}Tc inside waste forms [60]. Both Fe (II) and S (II) become reactive reductants once they dissolve, and they can effectively reduce ^{99}Tc that may be present in the pore water to form more stable reduced Tc (IV). The superior reducing properties of both FeS and BFS in our study were confirmed by XANES data (Figure 7, Table 3). It was determined that the FeS additive provides the highest reduction of Re (VII) to Re (IV) compared to other additives, while BFS ranks second in reducing capacity. Furthermore, the addition of BFS provides the highest compressive strength for the MKP specimens (Figure 6), indicating the formation of a denser structure compared to specimens modified with Fe_2O_3, Fe_3O_4, Fe, and FeS.

3. Materials and Methods

3.1. Raw Materials

Magnesium oxide (MgO) and potassium dihydrogen phosphate KH_2PO_4, both ≥98% purity, manufactured by Carl Roth®, Karlsruhe, Germany, were used to synthesis MKP-based matrices according to Equation (1). The MgO was calcined at 1200 °C for 2 h in air to reduce reactivity. Boric acid (H_3BO_3) with a purity of >99% (provided by Penta Chemicals Unlimited Co., Prague, Czech Republic) was added as a setting retarder. Rhenium oxide powder (Re_2O_7) with a purity of 99.9% (provided by Sigma-Aldrich®, St. Louis, MO, USA) was used as a source of rhenium.

The modifying Fe-bearing fillers were used during preparation of MKP-based specimens. The following powders were used as fillers: hematite (Fe_2O_3) provided by Sigma-Aldrich® s.r.o., Prague, Czech Republic; magnetite (Fe_3O_4), provided by Thermo Fisher GmbH, Kandel, Germany; metallic iron (Fe), provided by Sigma-Aldrich®, Stockholm, Sweden; iron sulfide (FeS), provided by Lachema N. P. Brno, Czech Republic; and BFS, in which the chemical composition is presented as: CaO (25–40) wt.%, SiO_2 (30–40) wt.%, Al_2O_3 (10–20) wt.%, MgO (1–5) wt.%, FeO (1–2) wt.% (provided by Moravia Steel, Trinec, Czech Republic).

The choice of fillers was determined by the desire to improve the properties of the matrices, but also by the fact that iron ions, also present in BFS, are capable of effectively

stabilizing ^{99}Tc in nuclear waste, reducing it from oxidation state (VII) to (IV), as described in the Introduction.

3.2. Specimen Preparation

In the present study, to obtain MKP-based matrices in accordance with Equation (1), a magnesium oxide (MgO)-to phosphate-(KH_2PO_4) molar ratio (M/P) of 2.25 and a water-to-cement mass ratio (W/C) of 0.5 were used, which were previously proposed for the immobilization of minor actinides [45]. Re_2O_7 (5 wt.%) was introduced into a dry mixture of MgO with KH_2PO_4. The laboratory process for obtaining MKP specimens is shown in Figure 9.

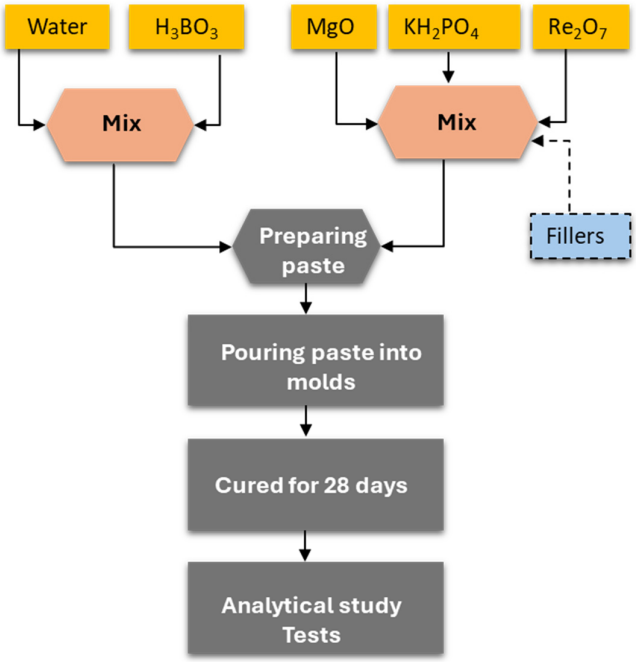


Figure 9. Scheme of the experimental procedure for obtaining MKP-based specimens with incorporated Re.

Dry raw components (MgO, KH_2PO_4, Re_2O_7) were initially weighed and then mixed in an Alpine Augsburg (Germany) lab grinding mill machine for 10 min according to the mixing proportions. Then, H_3BO_3 (5% of the MgO and KH_2PO_4 mass) was dissolved in deionized water. The dry component mixture was added to this solution, stirred mechanically for 3 min, and poured into (3 × 3 × 3 cm) plastic molds. These were tightly closed to avoid desiccation and air-cured for 1, 7, and 28 days at room temperature (20–25 °C). Fillers were added at the stage of preparing the dry powder mixture, and the studied basis proportions are presented in Table 5.

Table 5. Specimen powder proportions.

Batch	Dry Powder Mix Proportion (wt.%)						
	MgO + KH_2PO_4	**Re_2O_7**	**Fe_2O_3**	**Fe_3O_4**	**Fe**	**FeS**	**BFS**
MKP	100	0	0	0	0	0	0
MKP–Re	95	5	0	0	0	0	0
MKP–Re–Fe_2O_3	85	5	10	0	0	0	0
MKP–Re–Fe_3O_4	85	5	0	10	0	0	0
MKP–Re–Fe	85	5	0	0	10	0	0
MKP–Re–FeS	85	5	0	0	0	10	0
MKP–Re/BFS	85	5	0	0	0	0	10

Each filler (10 wt.%) was added based on references [61,62], in which the authors showed that the addition of various additives at 10 wt.% had a positive effect on increasing the strength of the magnesium phosphate-based compound.

3.3. Experimental Methods

3.3.1. Strength Test

The mechanical strength of MKP-based specimens (3 × 3 × 3 cm) after various curing periods was estimated by measuring the compressive strength with the use of a MEGA II-600 DMI-S (FORM+TEST Seidner & Co. GmbH, Riedlingen, Germany) universal testing machine at a loading rate of 0.25 MPa/s. The average compressive strength was determined by averaging the strength values of three MKP-based specimens.

3.3.2. Leaching Test

To assess the stability of the MKP matrix against leaching, the obtained MKP specimens were subjected to leaching tests according to ANSI/ANS-16.1 in deionized water for five leaching intervals at 1, 4, 14, 28, and 43 days (total 90 days) in a plastic vial at a room temperature. The volume of deionized water was 540 mL. The average effective diffusion coefficient D_e, often expressed in cm^2/s, was calculated from the ICP-MS concentration values measured for each leaching interval $t_n - t_{n-1}$ using this common expression:

$$D_e = \pi \left[\frac{a_n / A_0}{\Delta t_n} \right]^2 (V/S)^2 T \quad (4)$$

where V is the volume of the specimen (cm^3), S is the geometric surface area of the solid specimen (cm^2), a_n is the quantity of the element released from the specimen for the n'th leaching interval, A_0 is the initial quantity of the element in the specimen at the beginning of the first leaching interval, $\Delta t_n = t_n - t_{n-1}$ is the duration of the n'th leaching interval, and T is the leaching time representing the mean time of the leaching interval (s) as follows:

$$T = \left[\frac{1}{2} \left(\sqrt{t_n} - \sqrt{t_{n-1}} \right) \right]^2 \quad (5)$$

The leachability index (LI) of an element of concern in a material was defined as:

$$LI = \frac{1}{5} \sum_{1}^{5} \left[\log \left(\frac{\beta}{D_e} \right) \right] \quad (6)$$

where β is a constant (~1 cm^2/s).

The leachability index (LI) of an element is a parameter that suggests the effectiveness of the process for immobilization, and is used to regulate waste conditioning. According to the U.S. Nuclear Regulatory Commission (NRC) standard [59], the WAC for LI that is evaluated based on the ANSI/AN16.1 method should be greater than 6.0 to meet the requirement during the encapsulation process for radioactive waste conditioning.

3.3.3. Microstructural Analyses

The phase composition of MKP-based materials was determined using conventional Bragg–Brentano X-ray powder diffraction (XRD) measurements. Diffraction patterns were collected with a PANalytical X'Pert PRO diffractometer equipped with a conventional X-ray tube (CuK_α radiation, 40 kV, 30 mA, line focus) and a linear position-sensitive detector PIXCel with an anti-scatter shield. Qualitative analysis was performed with the High-ScorePlus software package (Malvern PANalytical, version 5.3.1) together with the PDF-5+

database [63]. Quantification of the experimental data was performed with the Rietveld method [64]. The Profex 4.3.6/BGMN 4.2.22 code was used for all calculations [65,66].

X-ray absorption spectroscopy was employed to determine the average oxidation state of Re in the specimens and to probe the local atomic environment around the Re absorber atoms. XANES spectra of the Re series were collected at the 10-ID-B beamline of the advanced photon source [67]. For measurements, each specimen was mixed with BN powder using a mortar and pestle to achieve a homogeneous mixture, which was then loaded into a 19 mm nylon washer and sealed with Kapton tape on both sides. The Re L_3 edge (10,534 eV) XANES spectra were collected in transmission mode, with each spectrum averaged from triplicate measurements. A Re metal foil was simultaneously measured as a reference. The collected spectra were processed using Athena from the Demeter software package (version 0.9.26) [68], running on the IFEFFIT algorithm, to perform reference foil measurement energy alignment and normalization. The absorption edge position (E_0) for the Re L_3 edge was defined as the zero-crossing point of the second derivative of each absorption curve.

The surface morphology and structure of specimens were analyzed by SEM with X-ray energy-dispersive spectroscopy (EDS) using a JSM-6510 microscope with an X-act-10 mm^2 SDD (JEOL Ltd., Tokyo, Japan) and a Talos F200X (Thermo Fisher Scientific Inc., Waltham, MA, USA) for TEM.

Raman spectroscopy was performed on a DXR Raman spectrometer (Thermo Fisher Scientific Inc., Waltham, MA, USA). The spectral range used to characterize MKP materials was between 0 and 3600 cm^{-1}.

4. Conclusions

In this study, the effects of iron-bearing additives (Fe_2O_3, Fe_3O_4, Fe, FeS and BFS) on the mechanical properties and water resistance of MKP-based specimens containing non-radioactive Re as a chemical analogue of long-lived radionuclide ^{99}Tc were investigated. Combining the results of XRD, Raman spectroscopy, SEM, TEM, XANES, and mechanical and leaching tests, the essential findings were as follows.

(1) The phase composition of the MKP-based matrix without iron-bearing additives changes upon the addition of 5 wt.% powdered Re_2O_7: in addition to K-struvite (77%) and periclase (16%), a new phase appears—potassium perrhenate or potassium rhenium oxide ($KReO_4$) (7%). In this case, a slight increase in the lattice parameters of K-struvite was observed, which led to an increase in the unit cell volume ($\Delta V = 0.13\%$) compared to pure MKP, which may indicate a partial inclusion of rhenium in the crystal lattice of K-struvite, given its ability for numerous substitutions. It was found that $KReO_4$ particles are characterized by a wide size distribution (up to 5 μm as a maximum) and are embedded in the MKP matrix. Therefore, the K-struvite matrix surrounds the $KReO_4$ particles and hinders the contact of Re (accordingly for Tc also) with the external environment, ensuring its immobilization in stable/durable waste form.

(2) The use of iron-bearing additives in the initial powder mixture (MKP + 5 wt.% Re_2O_7) had a positive effect on the mechanical properties of the resulting solid specimens. The measured compressive strengths of the matrices prepared with the addition of 10 wt.% Fe_2O_3, Fe_3O_4, Fe, FeS, and BFS after 28 days of curing were 37.8, 39.4, 37.1, 35.9, and 49.6 MPa, respectively, indicating an improvement over the initial strength (34 MPa) without additives.

(3) The oxidation state of Re in the presence of the reducing agent, such as Fe_2O_3, Fe_3O_4, Fe, FeS, and BFS, was preliminary revealed. The results of measurements using XANES can be interpreted as Re (VII), as a predominant oxidation state. At the same time, we can talk about a possible reduction process, which was confirmed by the

detection of a mix of oxidation states—possibly Re (VI) and/or Re (IV) mixed with Re (VII). The general trend in reduction state is this: FeS (highest), BFS, Fe, Fe_3O_4, Fe_2O_3 (lowest).

(4) Addition of iron-bearing fillers to the MKP-based matrix improves its water resistance, as evidenced by the results of leaching tests according to the ANSI/AN16.1 standard. The leachability index (LI) for Re from the MKP matrix prepared using the BFS additive was a maximum of 9.31, which meets the target LI > 9. This confirms the effectiveness of the waste form based on MKP with the addition of BFS for the Tc encapsulation process. Further research is ongoing to determine the optimal amount of BFS additive that will provide the greatest positive effect in preventing Re leaching from the MKP matrix.

Author Contributions: Conceptualization, H.-C.z.L., P.V. and S.S.; methodology, V.S. and V.K.; formal analysis, V.K., P.B. and S.S.; investigation, V.S., M.K., V.M., J.Š., N.M., P.E., S.T.M. and I.M.; writing—original draft, S.S.; writing—review and editing, H.-C.z.L. and P.V. All authors have read and agreed to the published version of the manuscript.

Funding: Research was conducted by the Center for Hierarchical Waste Form Materials (CHWM), an Energy Frontier Research Center (EFRC). Research was supported by the U.S. Department of Energy, Office of Basic Energy Sciences, Division of Materials Sciences and Engineering under Award DE-SC0016574. The research was carried out within the framework of the "UofSC-UJV Subaward No: 23-5123 Supporting Research to Develop TRU-Containing Phosphates for the Immobilization of Radioactive Elements," 2022–2024. This work was supported by Research Infrastructure NanoEnviCz, supported by the Ministry of Education, Youth and Sports of the Czech Republic under Project LM2023066.

Institutional Review Board Statement: Not applicable.

Informed Consent Statement: Not applicable.

Data Availability Statement: The original contributions presented in the study are included in the article. Further inquiries can be directed to the corresponding authors.

Acknowledgments: The Ukrainian authors are grateful to their Czech colleagues for the opportunity to work at UJV from mid-2022 since the war with Russia began in Ukraine. The research conducted at the beamline 10-ID-B used resources of the Advanced Photon Source, a U.S Department of Energy (DOE) Office of Science User Facility operated for the DOE Office of Science by Argonne National Laboratory under contract DE-AC02-06CH11357.

Conflicts of Interest: Authors Sergey Sayenko, Volodymyr Shkuropatenko, Petr Vecernik, Monika Kiselova, Vlastislav Kašpar and Vlastimil Miller were employed by the company ÚJV Řež, a. s., Nuclear Research Institute. The remaining authors declare that the research was conducted in the absence of any commercial or financial relationships that could be construed as a potential conflict of interest.

References

1. Meena, A.H.; Arai, Y. Environmental geochemistry of technetium. *Environ. Chem. Lett.* **2017**, *15*, 241–263. [CrossRef]
2. Buck, E.; Hanson, B.; McNamara, B. The geochemical behavior of Tc, Np and Pu in spent nuclear fuel in an oxidizing environment. In *Energy, Waste, and the Environment: Geochemical Perspective*; Giere, R., Stille, P., Eds.; Geological Society, Special Publications: London, UK, 2004; Volume 236, pp. 65–88.
3. Pearce, C.; Robert, C.; Moore, R.; Morad, W.; Matthew Asmussen, R.; Chatterjee, S.; Lawter, A.; Levitskaia, T.; Neeway, J.; Qafoku, N.; et al. Technetium immobilization by materials through sorption and redox-driven processes: A literature review. *Sci. Total Environ.* **2020**, *716*, 132849. [CrossRef]
4. Frederickson, J.K.; Zachara, J.M.; Kennedy, D.W.; Kukadapu, R.K.; McKinley, J.P.; Heald, S.M.; Liu, C.; Plymale, A.E. Reduction of $TcO4^-$ by sediment associated Fe(II). *Geochim. Cosmochim. Acta* **2004**, *68*, 3171–3187. [CrossRef]

5. Peretyazhko, T.S.; Zachara, J.M.; Kukadapu, R.K.; Heald, S.M.; Kutnyakov, I.V.; Resch, C.T.; Arey, B.W.; Wang, C.M.; Kovarik, L.; Phillips, J.L.; et al. Pertechnetate (TcO_4^-) reduction by reactive ferrous iron in naturally anoxic, redox transition zone sediments from the Hanford Site, USA. *Geochim. Cosmochim. Acta* **2012**, *92*, 48–66. [CrossRef]
6. Um, W.; Chang, H.; Icenhower, J.; Lukens, W.; Serne, R.; Qafoku, N.; Westsik, J.; Buck, E.; Smith, S. Immobilization of 99-Technetium (VII) by Fe(II)-Goethite and Limited Reoxidation. *Environ. Sci. Technol.* **2011**, *45*, 4904–4913. [CrossRef]
7. Um, W.; Chang, H.; Icenhower, J.; Lukens, W.; Serne, R.; Qafoku, N.; Kukkadapu, R.; Westsik, J. Iron oxide waste form for stabilizing ^{99}Tc. *J. Nucl. Mater.* **2012**, *429*, 201–209. [CrossRef]
8. Sayenko, S.; Shkuropatenko, V.; Vecernik, P.; Kašpar, V.; Kiselova, M.; Karsim, S.; Kolodiy, I.; Mateychenko, P.; Lobach, K.; Zykova, A. The effect of Fe_2O_3 and Fe_2O_3/Fe_3O_4 additives on the hydration, structure and strength of magnesium potassium phosphate cement for the immobilization radioactive wastes. *Probl. At. Sci. Technol.* **2025**, *2*, 61–70. [CrossRef]
9. Mayordomo, N.; Rodríguez, D.; Brendler, V.; Rossberg, A.; Scheinost, A.; Schild, D.; Cardaio, I.; Bureika, A.; Börner, C.; Müller, K. Immobilization of technetium by iron corrosion phases: Lessons learned and future perspectives. *Saf. Nucl. Waste Disposal* **2023**, *2*, 155–156. [CrossRef]
10. Liu, D.; Fan, X. Adsorption behavior of ^{99}Tc on Fe, Fe_2O_3 and Fe_3O_4. *J. Radioanal. Nucl. Chem.* **2005**, *264*, 691–698. [CrossRef]
11. Katheras, A.; Krack, M.; Zimmermann, T.; Scheinost, A.; Churakov, S. Incorporation Mechanism of Tc (IV) in Magnetite Revealed by EXAFS Measurements and Ab Initio Simulations. *J. Phys. Chem. C* **2025**, *129*, 5921−5930. [CrossRef]
12. Singh, B.K.; Mahzan, N.S.; Rashid, N.S.A.; Isa, S.A.; Hafeez, M.A.; Saslow, S.; Wang, G.; Mo, C.; Um, W. Design and Application of Materials for Sequestration and Immobilization of ^{99}Tc. *Environ. Sci. Technol.* **2023**, *57*, 6776–6798. [CrossRef]
13. Singh, B.K.; Kim, J.; Pak, D.; Kim, K.; Um, W. Technetium (Tc)/Rhenium (Re) solubility and leaching behavior from waste forms: An overview. *Front. Nucl. Eng.* **2023**, *1*, 1112080. [CrossRef]
14. Kim, E.; Boulègue, J. Chemistry of rhenium as an analogue of technetium: Experimental studies of the dissolution of rhenium oxides in aqueous solutions. *Radiochim. Acta* **2003**, *91*, 211–216. [CrossRef]
15. Kim, D.; Kruger, A.A. Volatile species of technetium and rhenium during waste vitrification. *J. Non-Cryst. Solids* **2018**, *481*, 41–50. [CrossRef]
16. Duckworth, S.; Gaona, X.; Castaño, D.; Park, S.; Altmaier, M.; Geckeis, H. Redox chemistry, solubility and hydrolysis of Re in reducing aquatic systems. Thermodynamic description and comparison with Tc. *Appl. Geochem.* **2021**, *132*, 105037. [CrossRef]
17. Arai, Y.; Meena, A.; Brain Lenell, B.; Powell, B.; Kaplan, D. Spatial distribution, chemical state, solubility of rhenium in a reducing cement waste form: Implications for predicting technetium mobility in saltstone. *Appl. Geochem.* **2017**, *85*, 180–187. [CrossRef]
18. Darab, J.G.; Smith, P.A. Chemistry of Technetium and Rhenium during Low-Level Radioactive Waste Vitrification. *Chem. Mater.* **1996**, *8*, 1004–1021. [CrossRef]
19. Kamorny, D.A.; Safonov, A.V.; Boldyrev, K.A.; Abramova, E.S.; Tyupina, E.A.; Gorbunova, O.A. Modification of the cement matrix with organic additives for stabilizing pertechnetate ions. *J. Nucl. Mater.* **2021**, *557*, 153295. [CrossRef]
20. Santikari, V.; Witmer, M.; Murdoch, L.C.; Kaplan, D.I.; Powell, B.A. Leaching and transport of technetium from reducing cementitious waste forms in field lysimeters. *Sci. Total Environ.* **2022**, *841*, 156596. [CrossRef] [PubMed]
21. Gartner, E. Industrially interesting approaches to "low-CO_2" cements. *Cem. Concr. Res.* **2004**, *34*, 1489–1498. [CrossRef]
22. Shi, C.; Jimenez, A.F.; Palomo, A. New cements for the 21st century: The pursuit of an alternative to Portland cement. *Cem. Concr. Res.* **2011**, *41*, 750–763. [CrossRef]
23. Garcia-Lodeiro, I.; Chhaiba, S.; Husillos-Rodriguez, N.; Palomo, Á.; Kinoshita, H. Development of Magnesium Phosphate Cement Based on Low-Grade MgO. *Materials* **2025**, *18*, 1198. [CrossRef] [PubMed]
24. Covill, A.; Hyatt, N.C.; Hill, J.; Collier, N.C. Development of magnesium phosphate cements for encapsulation of radioactive waste. *Adv. Appl. Ceram.* **2011**, *110*, 151–156. [CrossRef]
25. Xu, Q.; Chen, D.; Xiong, J.; He, X.; Dong, S.; Ma, L.; Hai, C.; Zhou, Y.; Sun, Y.A. Comprehensive Review of Advances in Magnesium-Based Cementitious Materials: Hydration, Properties, and Applications in Soil Stabilization. *Materials* **2025**, *18*, 3806. [CrossRef]
26. Wilson, A.; Nicholson, J. *Acid-Base Cements: Their Biomedical and Industrial Applications*; Cambridge University Press: Cambridge, UK, 2009. [CrossRef]
27. Xu, C.; Han, J.; Yang, Y. A review on magnesium potassium phosphate cement: Characterization methods. *J. Build. Eng.* **2024**, *82*, 108284. [CrossRef]
28. Mathew, M.; Schroeder, L.W. Crystal structure of a struvite analogue, $MgKPO_4 \cdot 6H_2O$. *Acta Crystallogr.* **1979**, *35*, 11–13. [CrossRef]
29. Gardner, L.; Bernal, S.; Walling, S.; Corkhill, C.; Provis, J.; Hyatt, N. Characterisation of magnesium potassium phosphate cements blended with fly ash and ground granulated blast furnace slag. *Cem. Concr. Res.* **2015**, *74*, 78–87. [CrossRef]
30. Westsik, J.H.; Cantrell, K.J.; Serne, R.J.; Qafoku, N.P. *Technetium Immobilization Forms Literature Survey*; Report PNNL-23329 EMSP-RPT-023, 4.4 Phosphate-Bonded Ceramics; U.S. Department of Energy: Washington, DC, USA, 2014.
31. Wagh, A.S. Chemically Bonded Phosphate Ceramics. In *Twenty-First Century Materials with Diverse Applications*, 2nd ed.; Elsevier: New York, NY, USA, 2016.

32. Qiao, F.; Chau, C.K.; Li, Z. Property evaluation of magnesium phosphate cement mortar as patch repair material. *Constr. Build. Mater.* **2010**, *24*, 695–700. [CrossRef]
33. Liu, K.; Ma, S.; Zhang, Z.; Han, F. Hydration and Properties of Magnesium Potassium Phosphate Cement Modified by Granulated Blast-Furnace Slag: Influence of Fineness. *Materials* **2022**, *15*, 918. [CrossRef]
34. Tan, Y.; Yu, H.; Li, Y.; Bi, W.; Yao, X. The effect of slag on the properties of magnesium potassium phosphate cement. *Constr. Build. Mater.* **2016**, *126*, 313–320. [CrossRef]
35. Wagh, A.S.; Jeong, S.Y. Chemically Bonded Phosphate Ceramics: I, A Dissolution Model of Formation. *J. Am. Ceram. Soc.* **2003**, *86*, 1838–1844. [CrossRef]
36. Singh, D.; Jeong, S.Y.; Dwyer, K.; Abesadze, T. Ceramicrete: A Novel Ceramic Packaging System for Spent-Fuel Transport and Storage. In Proceedings of the Waste Management 2K Conference, Tucson, AZ, USA, 27 February–2 March 2000.
37. Mattigod, S.V.; Lindberg, M.J.; Westsik, J.H.; Parker, K.E.; Chung, C.W. Waste Acceptance Testing of Secondary Waste Forms: Cast Stone, Ceramicrete and DuraLith. Report PNNL-20632, Contract DE-AC05-76RL01830; 2011. Available online: https://www.pnnl.gov/main/publications/external/technical_reports/PNNL-20632.pdf (accessed on 1 January 2026).
38. Vinokurov, S.E.; Kulyako, Y.M.; Slyunchev, O.M.; Rovnyi, S.I.; Wagh, A.S.; Maloney, M.D.; Myasoedov, B.F. Magnesium potassium phosphate matrices for immobilization of high-level liquid wastes. *Radiochemistry* **2009**, *51*, 65–72. [CrossRef]
39. Vinokurov, S.E.; Kulyako, Y.M.; Slyunchev, O.M.; Rovny, S.I.; Myasoedov, B.F. Low-temperature immobilization of actinides and other components of high-level waste in magnesium potassium phosphate matrices. *J. Nucl. Mater.* **2009**, *385*, 189–192. [CrossRef]
40. Singh, D.; Mandalika, V.; Parulekar, S.; Wagh, A. Magnesium potassium phosphate ceramic for ^{99}Tc immobilization. *J. Nucl. Mater.* **2006**, *348*, 272–282. [CrossRef]
41. Cantrell, K.; Um, W.; Williams, B.; Bowden, M.; Gartman, B.; Lukens, W.; Buck, E.; Mausolf, E. Chemical stabilization of Hanford tank residual waste. *J. Nucl. Mater.* **2014**, *446*, 246–256. [CrossRef]
42. Abramova, E.; Safonov, A.; Popova, N.; Kulikova, S.; Tyupina, E.; Vinokurov, S. Stability of modified technetium-containing magnesium potassium phosphate matrix under repository conditions with regard to biogeochemical effects. *Prog. Nucl. Energy* **2023**, *165*, 104902. [CrossRef]
43. Wagh, A.S.; Sayenko, S.Y.; Shkuropatenko, V.A.; Tarasov, R.V.; Dykiy, M.P.; Svitlychniy, Y.O.; Virych, V.D.; Ulybkina, E.A. Experimental Study on Cesium Immobilization in Struvite Structures. *J. Hazard. Mater.* **2016**, *302*, 241–249. [CrossRef]
44. Sayenko, S.Y.; Shkuropatenko, V.A.; Pylypenko, O.V.; Karsim, S.O.; Zykova, A.V.; Kutnii, D.V.; Wagh, A.S. Radioactive Waste Immobilization of Hanford Sludge in Magnesium Potassium Phosphate Ceramic Forms. *Prog. Nucl. Energy* **2022**, *152*, 104315. [CrossRef]
45. Loye, H.-C.Z.; Vecernik, P.; Kiselova, M.; Kašpar, V.; Korenkova, H.; Miller, V.; Bezdicka, P.; Šubrt, J.; Murafa, N.; Shkuropatenko, V.; et al. Investigation of Magnesium-Potassium Phosphates as Potential Nuclear Waste Form for the Immobilization of Minor Actinides. *Inorganics* **2024**, *12*, 311. [CrossRef]
46. Walling, S.; Provis, J. Magnesia-Based Cements: A Journey of 150 Years, and Cements for the Future? *Chem. Rev.* **2016**, *116*, 4180. [CrossRef]
47. Frost, R.; Weier, M.; Martens, W.; Henry, D.; Mills, S. Raman spectroscopy of newberyite, hannayite and struvite. *Spectrochim. Acta* **2005**, *62*, 181–188. [CrossRef]
48. Ishikawa, K.; Fujima, N.; Komura, H. First-order Raman scattering in MgO microcrystals. *J. Appl. Phys.* **1985**, *57*, 973. [CrossRef]
49. Li, M.-M.; Cao, J.-W.; Qin, X.-L.; Liu, X.-Y.; Yuan, X.-Q.; Dong, X.-T.; Guo, Q.; Sun, Y.; Zhang, P. Theoretical Prediction of Rhenium Separation from Ammonium Perrhenate by Phonon-Photon Resonance Absorption. *ACS Omega* **2022**, *7*, 5437–5441. [CrossRef] [PubMed]
50. Beattie, I.R.; Ozin, G.A. Vibrational Spectrum of Gaseous, Liquid, and Solid Re_2O_7. *J. Chem. Soc. (A) Inorg. Phys. Theor.* **1969**, 2615–2619. [CrossRef]
51. Xu, K.; Hrma, P.; Um, W.; Heo, J. Iron phosphate glass for immobilization of ^{99}Tc. *J. Nucl. Mater.* **2013**, *441*, 262–266. [CrossRef]
52. *Waste Form Technical Position, Revision 1*; Appendix A: B. Compression (A-3); US Nuclear Regulatory Commission: Washington, DC, USA, 1991. Available online: https://www.nrc.gov/docs/ML0336/ML033630746.pdf (accessed on 1 January 2026).
53. Byeon, H.; Jeong, G.; Park, J. Structural stability analysis of waste packages containing low- and intermediate-level radioactive waste in a silo-type repository. *Nucl. Eng. Technol.* **2021**, *53*, 1524–1533. [CrossRef]
54. EU Project PRE-DISposal Management of Radioactive Waste, Grant Agreement 945098: Deliverable 5.2. Report on Synthesis of Formulation & Process Studies Results. Final Version, 09/02/2024, p. 22. Available online: https://predis-h2020.eu/wp-content/uploads/2024/03/PREDIS_D5.2-Synthesis-report_vF-9.2.2024.pdf (accessed on 1 January 2026).
55. Sayenko, S.; Shkuropatenko, V.; Pylypenko, O.; Kholomieiev, H.; Karsim, S.; Zykova, A. Production and Properties of Magnesium Potassium Phosphate Cements Containing Ash and Metallurgical Slag Additives for Radioactive Waste Immobilization. *Nucl. Rad. Saf.* **2023**, *2*, 30–43. [CrossRef] [PubMed]
56. Zhang, Q.; Cao, X.; Ma, R.; Sun, S.; Fang, L.; Lin, J.; Luo, J. Solid waste-based magnesium phosphate cements: Preparation, performance and solidification/stabilization mechanism. *Constr. Build. Mater.* **2021**, *297*, 1237. [CrossRef]

57. Tougerti, A.; Cristol, S.; Berrier, E.; Briois, V.; Fontaine, C.; Villain, F.; Joly, Y. XANES study of rhenium oxide compounds at the L_1 and L_3 absorption edges. *Phys. Rev. B* **2012**, *85*, 125136. [CrossRef]
58. *ANSI/ANS-16.1*; Measurement of Leachability in Solidified Low-Level Radioactive Waste by the Short-Term Procedure—An American National Standard. American Nuclear Society: Westmont, IL, USA, 2019.
59. Tech/Position. U.S. Nuclear Regulatory Commission, Technical Position on Waste Form. Washington DC, 20555 Revision 1. Appendix A-7. 1991. Available online: www.nrc.gov/docs/ML0037/ML003752851.pdf (accessed on 1 January 2026).
60. Um, W.; Yang, J.; Serne, R.J.; Westsik, J. Reductive capacity measurement of waste forms for secondary radioactive wastes. *J. Nucl. Mater.* **2015**, *467*, 251–259. [CrossRef]
61. Liu, N.; Chen, B. Experimental research on magnesium phosphate cements containing alumina. *Constr. Build. Mater.* **2016**, *121*, 354–360. [CrossRef]
62. Ma, S.; Zhang, Z.; Liu, X.; Li, Y.; Zeng, Q.; Zhang, W. Reuse of red mud in magnesium potassium phosphate cement: Reaction mechanism and performance optimization. *Build. Eng.* **2022**, *61*, 105290. [CrossRef]
63. Kabekkodu, S.; Dosen, A.; Blanton, T. PDF-5+: A comprehensive Powder Diffraction File™ for materials characterization. *Powder Diffr.* **2024**, *39*, 47–59. [CrossRef]
64. Rietveld, H.M. A profile refinement method for nuclear and magnetic structures. *J. Appl. Crystallogr.* **1969**, *2*, 65–71. [CrossRef]
65. Bergmann, J.; Monecke, T.; Kleeberg, R. Alternative algorithm for the correction of preferred orientation in Rietveld analysis. *J. Appl. Crystallogr.* **2001**, *34*, 16–19. [CrossRef]
66. Döbelin, N.; Kleeberg, R. Profex: A graphical user interface for the Rietveld refinement program BGMN. *J. Appl. Crystallogr.* **2015**, *48*, 1573–1580. [CrossRef]
67. Segre, C.U.; Leyarovska, N.E.; Chapman, L.D.; Lavender, W.M.; Plag, P.W.; King, A.S.; Kropf, A.J.; Bunker, D.F.; Kemner, K.M.; Dutta, P.; et al. The MRCAT Insertion Device Beamline at the Advanced Photon Source. In *Proceedings of the Synchrotron Radiation Instrumentation, Stanford, CA, USA, 13–15 October 1999*; American Insitute of Physics: New York, NY, USA, 2000; pp. 419–422. [CrossRef]
68. Ravel, B.; Newville, M. ATHENA, ARTEMIS, HEPHAESTUS: Data analysis for X-ray absorption spectroscopy using IFEFFIT. *J. Synchrotron Radiat.* **2005**, *12*, 537–541. [CrossRef]

Disclaimer/Publisher's Note: The statements, opinions and data contained in all publications are solely those of the individual author(s) and contributor(s) and not of MDPI and/or the editor(s). MDPI and/or the editor(s) disclaim responsibility for any injury to people or property resulting from any ideas, methods, instructions or products referred to in the content.